

# Interface oscillations in reaction-diffusion systems beyond the Hopf bifurcation

Rebecca C. McKay\*, Theodore Kolokolnikov\* and Paul Muir†

\*Department of Mathematics and Statistics, Dalhousie University, Canada

†Department of Mathematics and Computing Science, Saint Mary's University, Canada

Abstract

We consider a reaction-diffusion system of the form

$$\begin{cases} u_t = \varepsilon^2 u_{xx} + f(u, w) \\ \tau w_t = D w_{xx} + g(u, w) \end{cases}$$

with Neumann boundary conditions on a finite interval. Under certain generic conditions on the nonlinearities  $f, g$  and in the singular limit  $\varepsilon \ll 1$  such a system may admit a steady state solution where  $u$  has sharp interfaces. It is also known that such interfaces may be destabilized due to a Hopf bifurcation [Y. Nishiura and M. Mimura. SIAM J. Appl. Math., 49:481–514, 1989], as  $\tau$  is increased beyond a certain threshold  $\tau_h$ . In this paper, we study what happens for  $\tau > \tau_h$ , or even  $\tau \rightarrow \infty$ , for a solution that consists of either one or two interfaces. Under the additional assumption  $D \gg 1$ , using singular perturbation theory, we determine the existence of another threshold  $\tau_c > \tau_h$  (where  $\tau_c$  is allowed to be infinite) such that if  $\tau_h < \tau < \tau_c$  then the system admits a solution consisting of periodically oscillating interfaces. On the other hand if  $\tau > \tau_c$ , the extent of the oscillation eventually exceeds the spatial domain size, even though very long transient dynamics can precede this occurrence. We make use of recently developed numerical software (that employs adaptive error control in space and time) to accurately compute an approximate solution. Excellent agreement with the analytical theory is observed.

## 1 Introduction

In this paper, we consider a reaction-diffusion system

$$\begin{cases} u_t = \varepsilon^2 u_{xx} + f(u, w) \\ \tau w_t = D w_{xx} + g(u, w) \end{cases} \quad (1)$$

in the limit

$$0 < \varepsilon \ll 1 \quad \text{and} \quad D \gg 1 \quad (2)$$

with  $\tau \geq 0$  and with Neumann boundary conditions on a bounded interval. Reaction-diffusion systems of the general form (1) have been widely used to model such diverse phenomena as chemical reactions [26, 40, 16, 21], gas discharge dynamics [10, 12], population dynamics [41, 1] and vegetation in arid landscapes [46]. Under certain conditions on the nonlinearities which will be described below, the solution for  $u$  consists of sharp interfaces that connect regions where  $u$  is nearly constant. A typical solution is shown in Figure 1(a,b). These solutions have been extensively studied and a large body of literature exists identifying their various properties. See for example [36, 29, 9, 32, 18, 17, 6, 39] and references therein.

An intriguing phenomenon that can occur for system (1) is the oscillatory or “breather” type behaviour, whereby interfaces exhibit a periodic motion in time. This is illustrated in Figure 1(e,f). Such

instability was first detected and analysed by Koga and Kuramoto for a reaction-diffusion system with piecewise cubic-type nonlinearity [20]. Since then, oscillatory behaviour was reported and analysed in many other reaction diffusion systems in one and higher dimensions, see for example [11, 13, 36, 10, 14, 15, 8, 33, 31, 45, 4, 12].

The onset of the oscillations for the system (1) is well understood in terms of a Hopf bifurcation. See for example [36, 20]. Typically, the Hopf bifurcation occurs when  $\tau$  is increased beyond a critical threshold  $\tau_h$  which can often be estimated analytically. However it is less clear what type of behaviour can be expected after the Hopf bifurcation threshold has been crossed. For  $\tau$  only slightly beyond  $\tau_h$ , weakly nonlinear analysis is possible [11, 10, 12]. In [11], the Hopf bifurcation structure was determined for a system of the form (1). More generally, in [10] the normal form for the oscillations close to the Hopf bifurcation in a generic reaction-diffusion system was identified. However the general form depends on certain constants which are not easily determined analytically. For a specific three-component gas model, this was further studied in [12], where it was determined that the Hopf bifurcation leading to the oscillatory behaviour can be either subcritical or supercritical, depending on parameter choice.

The main goal of this paper is to study *what happens as  $\tau$  is increased well beyond the Hopf bifurcation threshold  $\tau_h$* . In general, this is a difficult question, since such a problem lies beyond the weakly nonlinear regime. However here, we make the assumption that  $D$  is large. Unlike the previous works mentioned above, this critical assumption allows us to study the dynamics of the oscillatory fronts for *any*  $\tau$ , even if  $\tau$  is much bigger than  $\tau_h$ , and even for interface oscillations that are far away from equilibrium.

Our approach is inspired in part by [4], where the oscillation of spikes in the Gray-Scott model was analysed. There, the authors derived a reduced ODE-PDE Stephan problem with a moving source. By considering certain limits of the reduced problem, they re-obtained the Hopf bifurcation thresholds. Away from the Hopf bifurcation, they solved the Stephan problem numerically. We will follow a similar procedure: we start by obtaining a reduced ODE-PDE system for the motion of an interface of (1). However in contrast to [4], the assumption that  $D$  is large will allow us to further approximate the ODE-PDE system asymptotically by a weakly-forced harmonic oscillator, even far from the Hopf bifurcation.

Let us now describe the main results of this paper. While the derivation is done for the general system (1), for concreteness, we illustrate our results for the following cubic system (see for example [28, 9, 31]),

$$\begin{cases} u_t = \varepsilon^2 u_{xx} + 2(u - u^3) + w \\ \tau w_t = Dw_{xx} - u + \beta \end{cases} . \quad (3)$$

It is one of the simplest systems of the form (1) which admits interface solutions. In §2 we consider the initial conditions consisting of a single interface on  $x \in [0, 1]$ , such as shown in Figure 1(a). For the system (3), such a solution has the leading-order profile  $u(x, t) \sim \tanh((l(t) - x)/\varepsilon)$ ;  $w \sim 0$  where  $l(t)$  represents the interface position that changes slowly with time. The dotted line in Figure 1(c,e) shows the oscillation envelope which will be derived in Principal Result 2.1 for the general system (1). It agrees very well with the numerical solution of (3). The critical scaling for  $\tau$  turns out to be

$$\tau = \frac{D}{\varepsilon} \tau_0, \quad \text{where } \tau_0 \text{ is an } O(1) \text{ constant.}$$

The interface position is given by  $l(t) \sim l_0 + A(\hat{t}) \cos(\sqrt{3/\tau_0} \phi(t) + \phi_0)$ . Here,  $l_0$  is the position of the interface at the equilibrium given by  $l_0 = (1 + \beta)/2$ ; the envelope  $A$  evolves along the slow time scale  $\hat{t} = \varepsilon D^{-1} t$  whereas the frequency of the individual oscillations is along a faster but still slow time scale of  $\phi = \varepsilon D^{-1/2} t$ ;  $\phi_0$  is a constant. The initial conditions  $A(0)$  and  $\phi_0$  are determined by the initial positions of  $l(0)$  and  $w(l(0), 0)$ , and the oscillation envelope  $A$  satisfies the ODE

$$\frac{dA}{d\hat{t}} = \left( \frac{1}{4}(1 - 3\beta^2) - \frac{1}{8\tau_0} \right) A - \frac{3}{4} A^3. \quad (4)$$

The Hopf bifurcation threshold for  $\tau$  can then be easily determined by looking at the sign of the expression in brackets in (4). It is clearly negative for small (but positive)  $\tau_0$  but crosses zero when  $\tau = \tau_h = \frac{D}{\varepsilon} \tau_{0h}$  with  $\tau_{0h}$  given by

$$\tau_{0h} = \begin{cases} \frac{1}{2(1-3\beta^2)} & \text{if } |\beta| < 3^{-1/2}; \\ \infty & \text{otherwise} \end{cases} .$$

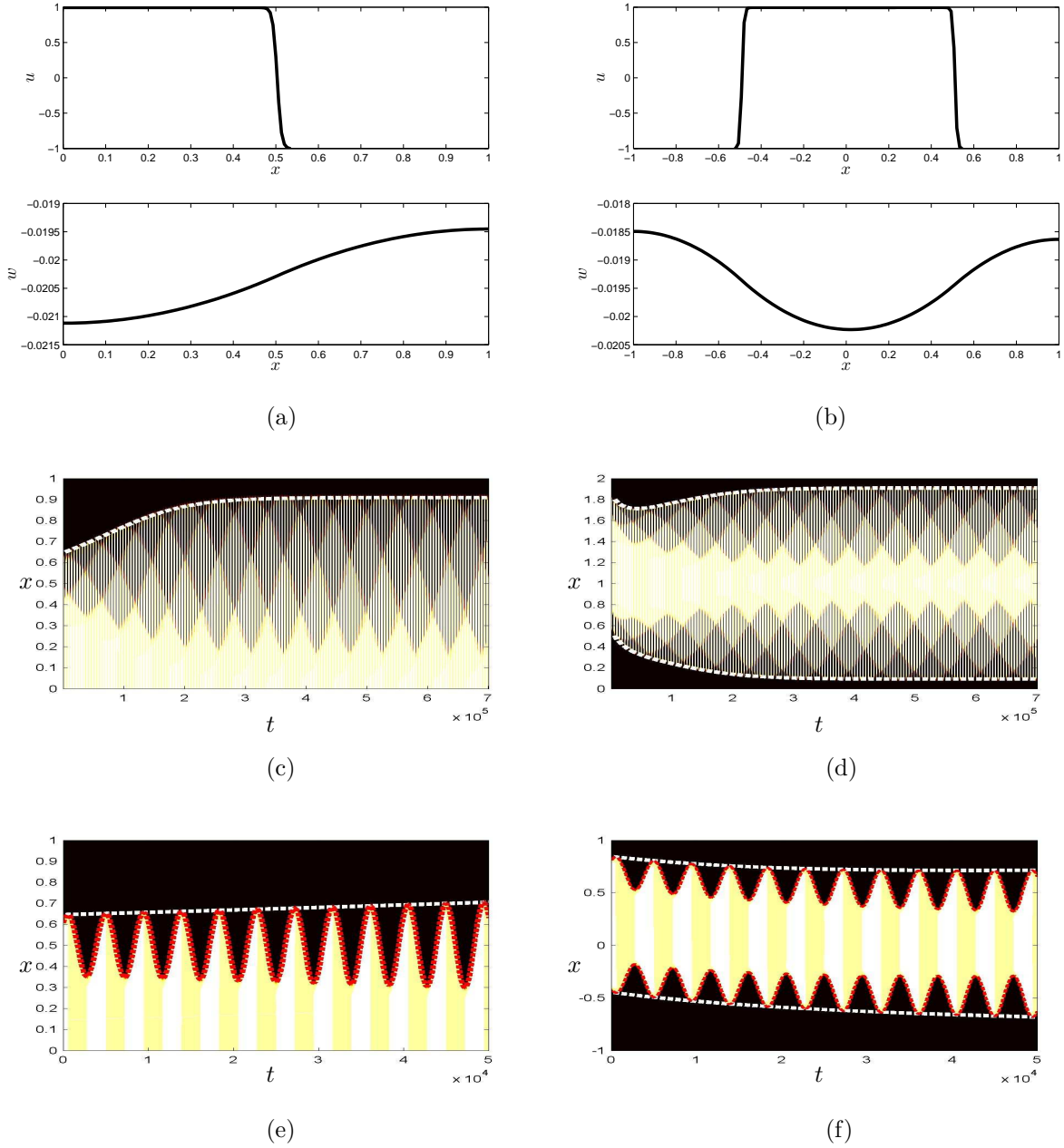


Figure 1: Simulations of the cubic model (3) with  $\beta = 0$ ,  $\varepsilon = 0.01$ ,  $D = 150$  and  $\tau = D/\varepsilon$ , that is,  $\tau_0 = 1.0$ . Left column shows the solution consisting of a single interface on the domain  $[0, 1]$ . Right column shows a two-interface solution on the domain  $[-1, 1]$ . (a) The snapshot of  $u$  and  $w$  at time  $t = 55001$ . Initial conditions consisted of a single interface located at  $l(0) = 0.6$ . (c) The contour plot of  $u$  showing the oscillation of the interface in time. Dark colour corresponds to  $u \approx -1$  and light to  $u \approx +1$ . The dashed white line denotes the amplitude of the oscillation as determined from our asymptotic results. (e) Zoom of (c) where  $l(t)$ , the location of the interface, is denoted by the dashed red line. (b,d,f): similar to (a,c,d) but for two-interface solution on the domain  $[-1, 1]$ . Initial conditions consisted of two interfaces located at  $-0.4$  and  $0.8$ .

For  $\tau_0 < \tau_{0h}$ , the interface settles at the position  $l \sim l_0$  whereas for  $\tau_0 > \tau_{0h}$ , the interface exhibits a periodic motion that converges to  $l \sim l_0 + A_\infty \cos(\sqrt{3/\tau_0}\phi + \phi_0)$  after a long transient period, where  $A_\infty$  is given by (95), and provided that  $l$  remains within the domain; that is  $l_0 + A_\infty < 1$  and  $l_0 - A_\infty > 0$  (if  $|\beta| > 3^{-1/2}$  then there is no Hopf bifurcation assuming  $\tau_0 > 0$ ). On the contrary case, the interface will eventually merge with the boundary after possibly a very long transient period. We note that these results hold even if  $\tau/\tau_h$  is not close to 1, and indeed we are able to capture the interface motion far from its equilibrium location.

For a more general system (1), we also show in Principal Result 2.1 that if  $|l_0 - \frac{1}{2}| < \frac{\sqrt{3}}{6}$ , there will always exist a Hopf bifurcation as  $\tau_0$  is increased. On the contrary case, the interface located at  $l_0$  is actually stable for all  $\tau > 0$ ; no Hopf bifurcation in  $\tau_0$  is possible. Similar analysis for the two interfaces of the general system (1) is given in Principal Result 3.1. In §4 we specialize these results to the system (3). We discuss the adaptive error control software that is used to integrate this model along very long time scales. This software is used to numerically integrate the full system (3). Despite the presence of two spatial and two temporal scales, we obtain excellent agreement between the analytical and numerical results. Finally in the discussion section §5 we make some further comments and suggest some open problems.

## 2 Oscillation of a single interface

In this section we consider the solution to (1) consisting of a single interface. We derive an equation for the amplitude of its oscillations. This allows us to obtain the Hopf bifurcation threshold, as well as to describe in detail the behaviour of solutions well beyond the Hopf bifurcation. The derivation of the amplitude equation is described in Principal Result 2.1. It consists of four steps. In the first step, we derive a reduced ODE-PDE system which describes the asymptotic motion of the interface in the original system (1). The reduced PDE is a Stefan-type heterogeneous linear diffusion equation, where the heterogeneity consists of Heaviside function which changes in time. This is coupled to an ODE which controls the position of the discontinuity in the Heaviside function. In the second step, we approximate the reduced ODE-PDE system by a 3rd order ODE system. We then approximate the 3rd order ODE by a weakly forced harmonic oscillator. Finally, we apply the method of multiple scales to derive the equations of motion for the amplitude  $A$ .

First, we introduce some notation. Define  $u_+$ ,  $u_-$  and  $w_0$  so that the following three equations are satisfied:

$$\int_{u_-}^{u_+} f(u, w_0) du = 0, \quad f(u_+, w_0) = 0 = f(u_-, w_0), \quad (5)$$

with  $u_+ \neq u_-$ . Define

$$g_\pm := g(u_\pm, w_0). \quad (6)$$

Suppose that  $f_u(u_\pm, w_0) < 0$  and  $0 < \frac{g_-}{g_- - g_+} < 1$ . Then a single interface steady state solution, on the interval  $[0, 1]$ , is given by

$$u(x) \sim U\left(\frac{x - l_0}{\varepsilon}\right), \quad w \sim w_0 \quad (7)$$

where  $U(y)$  is the heteroclinic connection between  $u_+$  and  $u_-$  satisfying

$$U_{yy} + f(U, w_0) = 0, \quad f(U(0), w_0) = 0 \quad (8)$$

$$U \rightarrow u_\pm \text{ as } y \rightarrow \mp\infty \quad (9)$$

and  $l_0$  is the equilibrium location of the interface given by

$$l_0 := \frac{g_-}{g_- - g_+} \quad (10)$$

so that

$$u \sim \begin{cases} u_+, & 0 < x < l_0, \\ u_-, & l_0 < x < 1. \end{cases} \quad (11)$$

This is a standard construction, see for example [28]. For convenience, we sketch it here. Consider a single interface located at  $x = l_0$  in the domain  $[0, 1]$ . We assume that  $u \sim u_+$  for  $0 < x < l_0$  and  $u \sim u_-$  for  $l_0 < x < 1$  where  $u_{\pm}$  are constants to be determined. Since it is assumed that  $D \gg 1$ , we expand

$$w = w_0 + \frac{1}{D}w_1 + \dots$$

so that to leading order  $w \sim w_0$  is a constant. Near the interface, we introduce the variables

$$x = l_0 + \varepsilon y; \quad u(x) \sim U\left(\frac{x - l_0}{\varepsilon}\right), \quad w \sim w_0.$$

Then  $U(y)$  satisfies (8) - (9). In order for such a solution to exist,  $u_+$  and  $u_-$  must be roots of  $f(u, w_0)$  and  $U$  must be a heteroclinic orbit connecting  $u_+$  and  $u_-$ . Therefore the constraints (5) determine  $u_+$ ,  $u_-$ , and  $w_0$ .

Integrating the second equation in (1) and recalling the boundary conditions  $w_x(0) = w_x(1) = 0$ , we obtain

$$\int_0^1 g(u, w_0) dx = 0.$$

Then, to leading order,

$$g_-(1 - l_0) + g_+l_0 = 0 \tag{12}$$

which yields (10).

Now we state the main result, describing the oscillation of the single interface.

**Principal Result 2.1** *Consider a single interface solution  $u$  of (1) in the limit (2) on the interval  $[0, 1]$  with Neumann boundary conditions. Let*

$$\tau = \frac{D}{\varepsilon}\tau_0 \tag{13}$$

Assume that

$$0 < l_0 < 1; \quad (g_- - g_+) \int_{u_-}^{u_+} f_w du > 0; \quad \left( g_w - \frac{f_w}{f_u} g_u \right) \Big|_{u=u_{\pm}, w=w_0} < 0, \tag{14}$$

where  $w_0, u_{\pm}, g_{\pm}$  and  $l_0$  are as defined by (5, 6, 10). Then the location of the interface  $l$  evolves according to

$$l(t) = l_0 + A(\hat{t}) \cos \left\{ \left( \frac{(g_- - g_+) \int_{u_-}^{u_+} f_w du}{\tau_0 \int_{-\infty}^{\infty} U_y^2 dy} \right)^{1/2} \phi + \phi_0 \right\} \tag{15}$$

where

$$\hat{t} = \frac{\varepsilon}{D}t; \quad \phi = \frac{\varepsilon}{\sqrt{D}}t; \tag{16}$$

$l_0$  is given by (10) and where  $A(\hat{t})$  is the amplitude of the oscillation of the interface, given by

$$\frac{dA}{d\hat{t}} = \frac{1}{2} \frac{\int_{u_-}^{u_+} f_w du}{\int_{-\infty}^{\infty} U_y^2 dy} \left\{ \hat{\sigma}_-(1 - l_0) + \hat{\sigma}_+l_0 - \frac{g_-^2 (6l_0^2 - 6l_0 + 1)}{3l_0^2(g_- - g_+)} \right\} A - \frac{(g_- - g_+) \int_{u_-}^{u_+} f_w du}{4 \int_{-\infty}^{\infty} U_y^2 dy} A^3 \tag{17}$$

where

$$\hat{\sigma}_{\pm} := \frac{1}{\tau_0} \frac{\int_{-\infty}^{\infty} U_y^2 dy}{\int_{u_-}^{u_+} f_w du} \left( g_w - \frac{f_w}{f_u} g_u \right) \Big|_{u=u_{\pm}, w=w_0}. \tag{18}$$

The initial conditions are determined by

$$A(0) \cos \phi_0 = l(0) - l_0, \quad -\sqrt{g_- - g_+} A(0) \sin \phi_0 = \sqrt{\tau_0 D} \left( \frac{\int_{u_-}^{u_+} f_w du}{\int_{-\infty}^{\infty} U_y^2 dy} \right)^{1/2} (w(0) - w_0). \tag{19}$$

Suppose that

$$\left| l_0 - \frac{1}{2} \right| < \frac{\sqrt{3}}{6}. \quad (20)$$

Then there exists a supercritical Hopf bifurcation occurs as  $\tau_0$  is increased past  $\tau_{0h}$  where

$$\tau_{0h} = \frac{3 \int_{-\infty}^{\infty} U_y^2 dy}{(g_- - g_+) \int_{u_-}^{u_+} f_w du} \frac{l_0 \left( g_w - \frac{f_w}{f_u} g_u \right) \Big|_{u=u_+} + (1 - l_0) \left( g_w - \frac{f_w}{f_u} g_u \right) \Big|_{u=u_-}}{(6l_0^2 - 6l_0 + 1)}, \quad (21)$$

Otherwise there is no Hopf bifurcation and  $A \rightarrow 0$  as  $\hat{t} \rightarrow \infty$  for any  $\tau_0 > 0$ .

**Derivation of Principal Result 2.1.** The derivation consists of a chain of reductions, whereby the original system (1) is first reduced to a coupled ODE-PDE system, then to a system of ODE, then to a weakly forced harmonic oscillator on which the method of multiple scales is applied to obtain the amplitude equations.

**Step 1:** We will first reduce (1) to an ODE-PDE system. We scale  $\tau$  as in (13) where  $\tau_0$  is  $\mathcal{O}(1)$ . Since we have assumed  $D \gg 1$ , we expand

$$u = u_0 + \frac{1}{D} u_1 + \dots, \quad w = w_0 + \frac{1}{D} w_1 + \dots.$$

For  $w$ , we have

$$w_{0,xx} = 0 \quad (22)$$

therefore, to leading order,  $w \sim w_0(t)$  is a constant in space. Expanding in terms of  $\frac{1}{D}$ , from the equation for  $u$  in (1), we obtain

$$0 = \varepsilon^2 u_{0,xx} + f(u_0, w_0), \quad (23)$$

$$D u_{0,t} = \varepsilon^2 u_{1,xx} + f_u(u_0, w_0) u_1 + f_w(u_0, w_0) w_1, \quad (24)$$

where  $u_{0,t} = \mathcal{O}\left(\frac{1}{D}\right)$  which will become evident with the scaling below. Consider a single interface located at  $x = l$  in the domain  $[0, 1]$ . Let  $l = l(t)$  and

$$u_0(x, t) = U\left(\frac{x-l}{\varepsilon}\right) = U(y) \quad (25)$$

where  $U$  is defined (7). Multiplying (24) by  $u_{0,x}$  and integrating by parts over the domain, we obtain

$$-l'(t) \int_0^1 u_{0,x}^2 dx = \frac{1}{D} \int_0^1 f_w w_1 u_{0,x} dx. \quad (26)$$

Note that the boundary terms from integration are negligible because  $u_0$  decays exponentially at the boundary. In the inner variables, we approximate  $w_1 \sim w_1(l)$ . Rearranging, we now have an equation for the dynamics of the interface

$$l_t = \frac{\varepsilon}{D} \frac{\int_{u_-}^{u_+} f_w du}{\int_{-\infty}^{\infty} U_y^2 dy} w_1(l).$$

Expanding in  $\frac{1}{D}$ , from the equation for  $w$  in (1), we obtain

$$\frac{\tau_0}{\varepsilon} w_{1,t} = w_{1,xx} + g(u_0, w_0) + \frac{1}{D} g_u(u_0, w_0) u_1 + \frac{1}{D} g_w(u_0, w_0) w_1 \quad (27)$$

Away from the interface, we can neglect the diffusion term,  $u_{1,xx}$ , so that

$$u_1 \sim -\frac{f_w(u_0, w_0)}{f_u(u_0, w_0)} w_1.$$

Then we have

$$\frac{\tau_0}{\varepsilon} w_{1_t} = w_{1_{xx}} + g(u_0, w_0) + \frac{1}{D} \left( g_w - \frac{f_w}{f_u} g_u \right) \Big|_{u=u_{\pm}, w=w_0} w_1.$$

Therefore, we obtain the following ODE-PDE system of  $l(t)$  and  $w_1(x, t)$

$$l_t = \frac{\varepsilon}{D} \frac{\int_{u_-}^{u_+} f_w du}{\int_{-\infty}^{\infty} U_y^2 dy} w_1(l), \quad (28)$$

$$\frac{\tau_0}{\varepsilon} w_{1_t} = w_{1_{xx}} + g(u_0, w_0) + \sigma w_1. \quad (29)$$

where

$$\sigma = \begin{cases} \sigma_+, & 0 < x < l \\ \sigma_-, & l < x < 1 \end{cases}, \quad (30)$$

with

$$\sigma_{\pm} = \frac{1}{D} \left( g_w - \frac{f_w}{f_u} g_u \right) \Big|_{u=u_{\pm}, w=w_0}. \quad (31)$$

Scaling the time variable and  $w_1$  allows us to clearly see that the ordering given above is consistent. Let this scaling be

$$s = \frac{\varepsilon}{\tau_0} \hat{\varepsilon} t; \quad \mathcal{W} = \hat{\varepsilon} w_1 \quad (32)$$

where

$$\hat{\varepsilon} = \sqrt{\frac{1}{D}} \left( \tau_0 \frac{\int_{u_-}^{u_+} f_w du}{\int_{-\infty}^{\infty} U_y^2 dy} \right)^{1/2}. \quad (33)$$

Then the scaled system is

$$l_s = \mathcal{W}(l), \quad (34)$$

$$\mathcal{W}_{xx} = \hat{\varepsilon} \mathcal{W}_s - \hat{\varepsilon} g(u_0, w_0) - \hat{\varepsilon}^2 \hat{\sigma} \mathcal{W}, \quad (35)$$

where

$$\hat{\sigma} = \begin{cases} \hat{\sigma}_+, & 0 < x < l \\ \hat{\sigma}_-, & l < x < 1 \end{cases} \quad (36)$$

with  $\hat{\sigma}_{\pm}$  as given by (18).

**Step 2.** In this step we reduce the ODE-PDE system (34, 35) to a system of three ODEs. Expanding  $\mathcal{W}$  in terms  $\hat{\varepsilon}$ ,

$$\mathcal{W} = \mathcal{W}_0(s) + \hat{\varepsilon} \mathcal{W}_1(x, s) + \hat{\varepsilon}^2 \mathcal{W}_2(x, s) + \dots, \quad (37)$$

we obtain

$$l_s = \mathcal{W}_0(s) + \hat{\varepsilon} \mathcal{W}_1(l, s), \quad (38)$$

$$\mathcal{W}_{0_{xx}} = 0, \quad (39)$$

$$\mathcal{W}_{0_s} = \mathcal{W}_{1_{xx}} + g_0, \quad (40)$$

$$\mathcal{W}_{1_s} = \hat{\sigma} \mathcal{W}_0 + \mathcal{W}_{2_{xx}}. \quad (41)$$

where

$$g_0 = \begin{cases} g_+, & x < l, \\ g_-, & x > l \end{cases} \quad (42)$$

with  $g_{\pm}$  as in (6). Equation (39) implies that  $\mathcal{W}_0 = \mathcal{W}_0(s)$ . From (40), we have the solvability condition

$$\int_0^1 \mathcal{W}_{1_{xx}} dx = \int_0^1 (\mathcal{W}_{0_s} - g_0) dx$$

so that

$$\mathcal{W}_{0_s} = \int_0^1 g_0 dx. = (g_+ - g_-)l - g_-, \quad (43)$$

and, from (40),

$$\mathcal{W}_{1_{xx}} = \begin{cases} \mathcal{W}_{0_s} - g_+, & x < l, \\ \mathcal{W}_{0_s} - g_-, & x > l. \end{cases} \quad (44)$$

Substituting (43) into (44), integrating and imposing continuity of  $\mathcal{W}_1$  at  $x = l$ , we obtain

$$\mathcal{W}_1 = \begin{cases} (g_+ - g_-)(l - 1) \left( \frac{x^2}{2} - \frac{l^2}{2} \right) + K(s), & x < l \\ (g_+ - g_-)l \left( \frac{x^2}{2} - x - \frac{l^2}{2} + l \right) + K(s), & x > l \end{cases}$$

where  $K(s)$  is to be determined as follows. From (41), we have the solvability condition

$$\int_0^1 \mathcal{W}_{1_s} dx = \int_0^1 \hat{\sigma} \mathcal{W}_0 dx$$

from which we can solve for  $K_s$ ,

$$K_s = (g_+ - g_-)l_s \left\{ 2l^2 - 2l + \frac{1}{3} \right\} + (\hat{\sigma}_+ - \hat{\sigma}_-) \mathcal{W}_0 l + \hat{\sigma}_- \mathcal{W}_0.$$

We then obtain a system of three ODE's that capture the interface motion,

$$l_s = \mathcal{W}_0(s) + \hat{\varepsilon} K(s), \quad (45)$$

$$\mathcal{W}_{0_s} = (g_+ - g_-)l + g_-, \quad (46)$$

$$K_s = \mathcal{W}_0 \left\{ (g_+ - g_-) \left( 2l^2 - 2l + \frac{1}{3} \right) + (\hat{\sigma}_+ - \hat{\sigma}_-)l + \hat{\sigma}_- \right\}. \quad (47)$$

**Step 3.** We now approximate the system (45, 46, 47) by a weakly linear oscillator. We start by changing the variables

$$l = l_0 + y = \frac{g_-}{g_- - g_+} + y \quad (48)$$

to shift the equilibrium of (46) to zero. Then

$$y_s = \mathcal{W}_0 + \hat{\varepsilon} K, \quad (49)$$

$$\mathcal{W}_{0_s} = (g_+ - g_-)y, \quad (50)$$

$$K_s = \mathcal{W}_0 \left\{ 2(g_+ - g_-)y^2 + (\hat{\sigma}_+ - \hat{\sigma}_-)y - 2(g_+ + g_-)y \right. \\ \left. \hat{\sigma}_-(1 - l_0) + \hat{\sigma}_+ l_0 - \frac{g_-^2 (6l_0^2 - 6l_0 + 1)}{3l^2(g_- - g_+)} \right\}. \quad (51)$$

Differentiating (49) and substituting (50) and (51), we obtain

$$y_{ss} = \mathcal{W}_{0_s} + \hat{\varepsilon} K_s \quad (52)$$

$$= (g_+ - g_-)y + \hat{\varepsilon} \mathcal{W}_0 \left\{ 2(g_+ - g_-)y^2 + (\hat{\sigma}_+ - \hat{\sigma}_-)y - 2(g_+ + g_-)y \right. \\ \left. \hat{\sigma}_-(1 - l_0) + \hat{\sigma}_+ l_0 - \frac{g_-^2 (6l_0^2 - 6l_0 + 1)}{3l^2(g_- - g_+)} \right\}. \quad (53)$$

$$\hat{\sigma}_-(1 - l_0) + \hat{\sigma}_+ l_0 - \frac{g_-^2 (6l_0^2 - 6l_0 + 1)}{3l^2(g_- - g_+)} \left. \right\}. \quad (54)$$

From (49) we have  $\mathcal{W}_0 = y_s + \mathcal{O}(\varepsilon)$ . Keeping only  $\mathcal{O}(1)$  and  $\mathcal{O}(\varepsilon)$  terms we then obtain

$$y_{ss} = (g_+ - g_-)y + \hat{\varepsilon}y_s \left\{ 2(g_+ - g_-)y^2 + (\hat{\sigma}_+ - \hat{\sigma}_-)y - 2(g_+ + g_-)y \right. \\ \left. \hat{\sigma}_-(1 - l_0) + \hat{\sigma}_+l_0 - \frac{g_-^2(6l^2 - 6l + 1)}{3l^2(g_- - g_+)} \right\} + \mathcal{O}(\varepsilon^2). \quad (55)$$

**Step 4.** Now, we perform a multiple scales analysis on (55), see for example [2]. We expand  $y(s) = y_0(s, \hat{\tau}) + \hat{\varepsilon}y_1(s, \hat{\tau}) + \dots$ , where  $\hat{\tau} = \varepsilon s$  is the slow variable. We then obtain, to two orders,

$$y_{0ss} + \omega^2 y_0 = 0, \quad (56)$$

$$y_{1ss} + \omega^2 y_1 = -2y_{0s\hat{\tau}} + (\hat{\sigma}_+ - \hat{\sigma}_-)y_0 y_{0s} - 2(g_+ + g_-)y_0 y_{0s} + 2(g_+ - g_-)y_0^2 y_{0s} \\ + \left\{ \hat{\sigma}_-(1 - l_0) + \hat{\sigma}_+l_0 - \frac{g_-^2(6l_0^2 - 6l_0 + 1)}{3l^2(g_- - g_+)} \right\} y_{0s} \quad (57)$$

where we defined

$$\omega := \sqrt{g_- - g_+}.$$

From (56) we obtain

$$y_0 = A(\hat{\tau}) \cos(\omega s + \phi(\hat{\tau})). \quad (58)$$

Eliminating the resonance terms from (57), we obtain the system of equations

$$2A \frac{d\phi}{d\hat{\tau}} = 0 \quad (59)$$

$$2 \frac{dA}{d\hat{\tau}} = - \left( \frac{g_- - g_+}{2} \right) A^3 + \left\{ \hat{\sigma}_-(1 - l_0) + \hat{\sigma}_+l_0 - \frac{g_-^2(6l_0^2 - 6l_0 + 1)}{3l^2(g_- - g_+)} \right\} A \quad (60)$$

Equation (59) implies  $\phi = \phi_0$  where  $\phi_0$  is a constant. Rewriting in terms of the original time variable  $t$ , the equation for the amplitude of the movement of the interface (60) yields

$$\frac{dA}{dt} = \frac{\varepsilon}{D} \frac{\int_{u_-}^{u_+} f_w du}{\int_{-\infty}^{\infty} U_y^2 dy} \left\{ \frac{-(g_- - g_+)}{4} A^3 + \frac{1}{2} \left\{ \hat{\sigma}_-(1 - l_0) + \hat{\sigma}_+l_0 - \frac{g_-^2(6l_0^2 - 6l_0 + 1)}{3l_0^2(g_- - g_+)} \right\} A \right\} \quad (61)$$

The initial condition  $A(0)$  and the constant  $\phi_0$  are determined from the initial conditions of the original problem (1), which yields the equations (19).

From (60), the bifurcation occurs when the coefficient of  $A$  in (17) changes from positive to negative. Setting it to zero and solving for  $\tau_0 = \tau_{0h}$  yields the expression (21). Assuming  $\tau_{0h} > 0$ , It is easy to verify that the term in the curly brackets in (17) is negative provided  $\tau < \tau_{0h}$  and provided that the assumption (14) holds. This implies that the bifurcation is supercritical. For  $\tau_0 > \tau_{0h}$ , the interface will oscillate in time and approach a constant amplitude. It remains to determine under which conditions  $\tau_{0h}$  given by (21) is actually positive. From (14),  $\tau_{0h}$  is positive whenever  $6l_0^2 - 6l_0 + 1 < 0$  which is precisely the condition (20). ■

We note that the oscillation of the interface must be contained in the domain  $[0, 1]$ . To satisfy this, we must have

$$l_0 + A < 1, \quad l_0 - A > 0.$$

This may impose additional thresholds on the parameters. We will discuss this further in the context of the cubic model (3) in Proposition 4.1.

### 3 Oscillations of two interfaces

Now we consider a a solution consisting of two interfaces for the general system (1). We state a similar result to that obtained in §2 for one interface.

**Principal Result 3.1** Consider a two-interface solution  $u$  of (1) in the limit (2) on the interval  $[-1, 1]$  with Neumann boundary conditions of the general form

$$u \sim \begin{cases} u_+, & x \in (x_l, x_r) \\ u_-, & x \in [-1, 1] \setminus (x_l, x_r). \end{cases}$$

and assume that (14) hold with  $w_0, u_{\pm}, g_{\pm}, l_0$  as defined in Principal Result 2.1. Here,  $x_l = x_l(t), x_r = x_r(t)$  are time-dependent locations of the left and right interface, respectively with  $-1 < x_l < x_r < 1$ . Define

$$x_0 := \frac{x_r + x_l}{2} \quad (62)$$

and

$$l := \frac{x_r - x_l}{2}. \quad (63)$$

Then  $l$  evolves according to

$$l(t) = l_0 + A(\hat{t}) \cos \left\{ \left( \frac{(g_- - g_+) \int_{u_-}^{u_+} f_w du}{\tau_0 \int_{-\infty}^{\infty} U_y^2 dy} \right)^{1/2} \phi + \phi_0 \right\}$$

where  $\hat{t}, \phi, \omega$  are as given in Principal Result 2.1 and  $A$  and  $x_0$  satisfy a coupled ODE system

$$\frac{dx_0}{d\hat{t}} = - \frac{(g_- - g_+) \int_{u_-}^{u_+} f_w du}{\int_{-\infty}^{\infty} U_y^2 dy} x_0 \left( \frac{A^2}{2} + l_0^2 \right) \quad (64)$$

$$\frac{dA}{d\hat{t}} = \frac{\int_{u_-}^{u_+} f_w du}{2 \int_{-\infty}^{\infty} U_y^2 dy} \left\{ \hat{\sigma}_- (1 - l_0) + \hat{\sigma}_+ l_0 - \frac{g_-^2 (6l_0^2 - 6l_0 + 1)}{3l_0^2 (g_- - g_+)} - (g_- - g_+) x_0^2 \right\} A - \frac{(g_- - g_+) \int_{u_-}^{u_+} f_w du}{4 \int_{-\infty}^{\infty} U_y^2 dy} A^3 \quad (65)$$

where  $\hat{\sigma}_{\pm}$  is defined as in (18). A supercritical Hopf bifurcation occurs when  $\tau_0 = \tau_{0h}$  where  $\tau_{0h}$  is given by (21).

From (64), we can see in the limit  $\hat{t} \gg 1, x_0 \rightarrow 0$  so that (65) becomes (17). Thus, the Hopf bifurcation occurs at the same critical  $\tau_0$  value as for the one interface case in (21). Since  $x_0 \rightarrow 0$ , the two-interface solution exhibits *in-phase* oscillations, that is, the oscillation is in the distance between interfaces. In [14], *out-of-phase* oscillations are also shown (see Figures 1.7, 1.10 and 1.11). These are not examined here. Further discussion of this is found in §5.

**Derivation of Principal result 3.1.** The derivation is similar to Principal Result 2.1; here we outline the main differences. As before, we scale  $\tau$  as (13) and we expand  $u = u_0 + \frac{1}{D} u_1 + \dots$  and  $w = w_0 + \frac{1}{D} w_1 + \dots$ . Similar to Principal Result 2.1, we then obtain the reduced ODE-PDE system,

$$x_{rt} = \frac{\varepsilon \int_{u_-}^{u_+} f_w du}{D \int_{-\infty}^{\infty} U_y^2 dy} w_1(x_r),$$

$$x_{lt} = - \frac{\varepsilon \int_{u_-}^{u_+} f_w du}{D \int_{-\infty}^{\infty} U_y^2 dy} w_1(x_r).$$

and

$$\frac{\tau_0}{\varepsilon} w_{1t} = w_{1xx} + g(u_0, w_0) + \sigma w_1$$

where  $\sigma$  and  $u_0$  is given by

$$\sigma = \begin{cases} \sigma_+, & x \in (x_l, x_r) \\ \sigma_-, & x \in (-1, x_l) \cup (x_r, 1) \end{cases}; \quad u_0 = \begin{cases} u_+, & x \in (x_l, x_r) \\ u_-, & x \in (-1, x_l) \cup (x_r, 1) \end{cases} \quad (66)$$

with  $\sigma_{\pm}$  given by (31). We scale  $t$  and  $w_1$  as before, in (32) where  $\hat{\varepsilon}$  is given by (33). Then

$$\begin{aligned}\mathcal{W}_{xx} &= \hat{\varepsilon}\mathcal{W}_s - \hat{\varepsilon}g(u_0, w_0) - \hat{\varepsilon}^2\hat{\sigma}\mathcal{W}, \\ x_{r_s} &= \mathcal{W}(x_r), \\ x_{l_s} &= -\mathcal{W}(x_l)\end{aligned}$$

where  $\hat{\sigma}$  is

$$\hat{\sigma} = \begin{cases} \hat{\sigma}_+, & x \in (x_l, x_r) \\ \hat{\sigma}_-, & x \in (-1, x_l) \cup (x_r, 1) \end{cases} \quad (67)$$

with  $\hat{\sigma}_{\pm}$  given in (18). Expanding  $\mathcal{W} = \mathcal{W}_0(x, s) + \hat{\varepsilon}\mathcal{W}_1(x, s) + \hat{\varepsilon}^2\mathcal{W}_2(x, s) + \dots$ , similar to (38)-(41), we now have the system

$$x_{r_s} = \mathcal{W}_0(s) + \hat{\varepsilon}\mathcal{W}_1(x_r, s), \quad (68)$$

$$x_{l_s} = -\mathcal{W}_0(s) - \hat{\varepsilon}\mathcal{W}_1(x_l, s), \quad (69)$$

$$\mathcal{W}_{0_s} = \mathcal{W}_{1xx} + g(u_0, w_0), \quad (70)$$

$$\mathcal{W}_{1_s} = \hat{\sigma}\mathcal{W}_0 + \mathcal{W}_{2_{xx}} \quad (71)$$

We integrate (70) over the domain to obtain

$$\mathcal{W}_{0_s} = (g_+ - g_-) \left( \frac{x_r - x_l}{2} \right) + g_-. \quad (72)$$

We rewrite  $x_l, x_r$  in terms of  $x_0, l$  as defined in (62, 63) so that

$$x_l = x_0 - l \quad \text{and} \quad x_r = x_0 + l.$$

Then in terms of  $l$  and  $x_0$  we obtain

$$x_{0_s} = \mathcal{W}_0 + \hat{\varepsilon}\mathcal{W}_1(x_0 + l, s) - l_s \quad (73)$$

$$l_s = \mathcal{W}_0 + \hat{\varepsilon}\mathcal{W}_0 + \hat{\varepsilon}(x_0 - l, s) - x_{0_s} \quad (74)$$

$$\mathcal{W}_{0_s} = (g_+ - g_-)l + g_- \quad (75)$$

$$\mathcal{W}_{1_s} = \hat{\sigma}\mathcal{W}_0 + \mathcal{W}_{2_{xx}} \quad (76)$$

As before, we integrate (70), impose continuity of  $\mathcal{W}_1$  at the interfaces  $x_l$  and  $x_r$ , and substitute (72) to obtain

$$\mathcal{W}_1 = \begin{cases} (g_+ - g_-)l \left( \frac{x^2}{2} + x \right) + (g_+ - g_-) \frac{(x_0 - l)^2}{2} + K(s), & -1 < x < x_0 - l \\ (g_+ - g_-)(l - 1) \left( \frac{x^2}{2} \right) + (g_+ - g_-)x_0x + K(s), & x_0 - l < x < x_0 + l \\ (g_+ - g_-)l \left( \frac{x^2}{2} - x \right) + (g_+ - g_-) \frac{(x_0 + l)^2}{2} + K(s), & x_0 + l < x < 1 \end{cases}$$

Integrating (76) over the domain, we have the solvability condition

$$\int_{-1}^1 (\mathcal{W}_{1_s} - \hat{\sigma}\mathcal{W}_0) dx = 0.$$

Solving this, we have the following equation

$$K_s = -\frac{1}{2}(g_+ - g_-)l_s \left( -x_0^2 - l^2 + 2l - \frac{2}{3} \right) - (g_+ - g_-)x_0x_{0_s}(1 - l) - \mathcal{W}_0(\hat{\sigma}_+l + \hat{\sigma}_-(l - 1)).$$

Thus, as for one interface, we obtain the following ODE system

$$x_{0_s} = \hat{\varepsilon}(g_+ - g_-)x_0l^2, \quad (77)$$

$$l_s = \mathcal{W}_0 + \hat{\varepsilon}\frac{1}{2}(g_+ - g_-)(x_0^2(l + 1) + l^3 - l^2) + \hat{\varepsilon}K(s), \quad (78)$$

$$\mathcal{W}_{0_s} = (g_+ - g_-)l + g_-, \quad (79)$$

$$K_s = \frac{1}{2}(g_- - g_+)l_s \left( -\frac{2}{3} - x_0^2 - l^2 + 2l \right) - (g_- - g_+)x_0x_{0_s}(l + 1) - \mathcal{W}_0(\hat{\sigma}_+l + \hat{\sigma}_-(l - 1)). \quad (80)$$

As before, we let  $l = l_0 + y$  to shift the equilibrium of (79) and eliminate the  $K$  and  $\mathcal{W}_0$  equations to obtain the approximate system

$$x_{0s} = \hat{\varepsilon}(g_+ - g_-)x_0(l_0 + y)^2 \quad (81)$$

$$y_{ss} = (g_+ - g_-)y + \hat{\varepsilon}y_s \left\{ 2(g_+ - g_-)y^2 + (\hat{\sigma}_+ - \hat{\sigma}_-)y - 2(g_+ + g_-)y - (g_- - g_+)x_0^2 + \hat{\sigma}_-(1 - l_0) + \hat{\sigma}_+l_0 - \frac{g_-^2(6l_0^2 - 6l_0 + 1)}{3l_0^2(g_- - g_+)} \right\} \quad (82)$$

We again follow with a multiple scales analysis. Let  $y = y_0(s, \hat{\tau}) + \hat{\varepsilon}y_1(s, \hat{\tau})$  where  $\hat{\tau} = \hat{\varepsilon}s$ . Also, expand  $x_0 = x_{00}(s, \hat{\tau}) + \hat{\varepsilon}x_{01}(s, \hat{\tau})$ . This expansion gives

$$x_{00s} = 0 \quad (83)$$

$$x_{01s} = -x_{00\hat{\tau}} - \omega^2 x_{00}(y_0 + l_0)^2 \quad (84)$$

$$y_{0ss} + \omega^2 y_0 = 0 \quad (85)$$

$$y_{1ss} + \omega^2 y_1 = -2y_{0s\hat{\tau}} + 2(g_+ - g_-)y_0^2 y_{0s} + ((\hat{\sigma}_+ - \hat{\sigma}_-) - 2(g_+ + g_-))y_0 y_{0s} + \left( \hat{\sigma}_-(1 - l_0) + \hat{\sigma}_+l_0 - (g_- - g_+)x_0^2 - \frac{g_-^2(6l_0^2 - 6l_0 + 1)}{3l_0^2(g_- - g_+)} \right) y_{0s} \quad (86)$$

where

$$\omega = \sqrt{g_- - g_+}.$$

From (85),  $y_0 = A(\hat{\tau}) \cos(\omega s + \phi(\hat{\tau}))$  and (83) implies that  $x_{00}(s, \hat{\tau}) = x_{00}(\hat{\tau})$ . Eliminating the resonance terms for  $x_{01}$  then yields

$$\frac{dx_{00}}{d\hat{\tau}} = -\omega^2 x_{00} \left( \frac{A^2}{2} + l_0^2 \right). \quad (87)$$

Eliminating the resonance terms in (85), we obtain

$$2 \frac{dA}{d\hat{\tau}} = - \left( \frac{g_- - g_+}{2} \right) A^3 + \left( \hat{\sigma}_-(1 - l_0) + \hat{\sigma}_+l_0 - (g_- - g_+)x_0^2 - \frac{g_-^2(6l_0^2 - 6l_0 + 1)}{3l_0^2(g_- - g_+)} \right) A \quad (88)$$

Rescaling, this completes the derivation of the Principal Result 3.1. ■

## 4 Numerical Simulations

To verify our asymptotic results, we simulate the full PDE system (1). In this section, we specialize the principal results of §2 and §3 to the particular case of the cubic model (3). Then we discuss the numerical software used in computing the solution to the PDE system. Finally, we compare numerically the solution of the PDE system with that of the asymptotic amplitude equations.

### 4.1 Applying Principal Results to the cubic model

We specialize our results to the system (3):

$$f(u, w) = 2(u - u^3) + w; \quad g(u, w) = \beta - u. \quad (89)$$

From (5) - (10) we obtain

$$w_0 = 0; \quad u_- = -1, \quad u_+ = +1; \quad U(y) = -\tanh(y); \quad (90)$$

$$g_+ = \beta - 1, \quad g_- = \beta + 1; \quad l_0 = \frac{1 + \beta}{2} \quad (91)$$

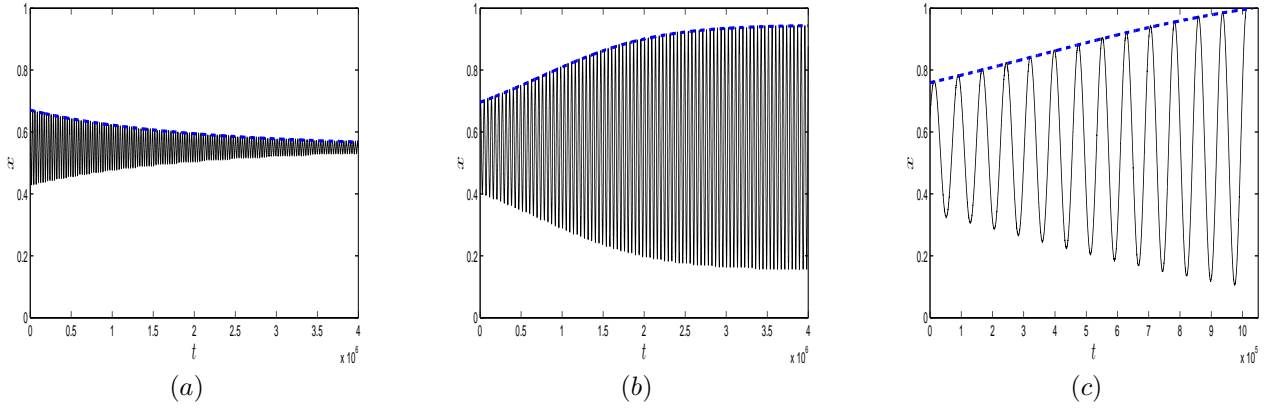


Figure 2: Comparison of numerical simulations of (3) with asymptotics. Parameter values are  $\beta = 0.1$ ,  $D = 150$ ,  $\varepsilon = 0.001$ ; initial conditions are given by (98). Dashed line indicates the oscillation envelope  $A(t)$ . Solid line indicates the location of the interface of the computed solution  $u(x, t)$ . (a)  $\tau_0 = 0.4$  (b)  $\tau_0 = 1$  (c)  $\tau_0 = 3$ . See Experiment 2 of §4

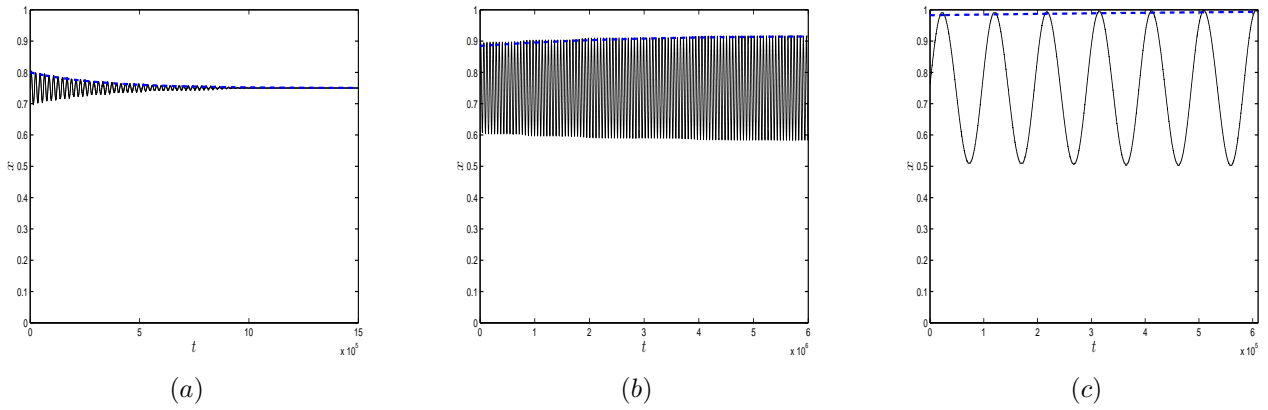


Figure 3: Comparison of numerical simulations of (3) with asymptotics. Parameter values are  $\beta = 0.5$ ,  $D = 80$ ,  $\varepsilon = 0.001$ ; initial conditions are given by (99). Dashed line indicates the oscillation envelope  $A(t)$ . Solid line indicates the location of the interface of the computed solution  $u(x, t)$ . (a)  $\tau_0 = 0.4$  (b)  $\tau_0 = 3$  (c)  $\tau_0 = 9$ . See Experiment 3 of §4

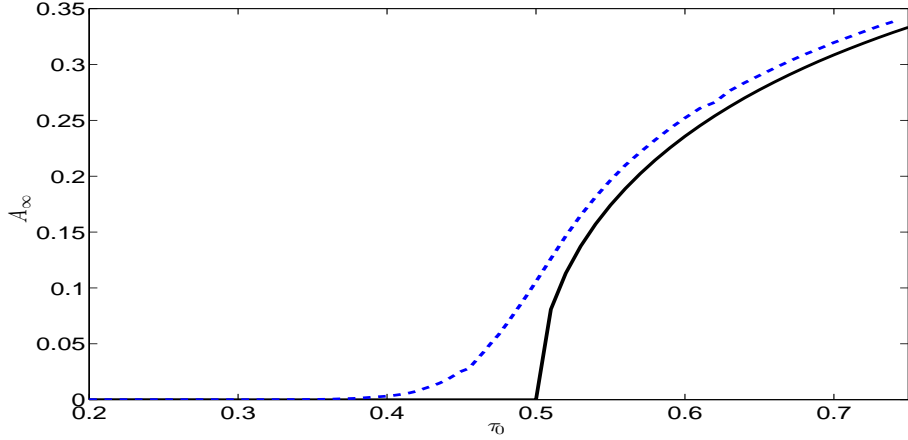


Figure 4: Comparison of  $A_\infty$  for the model (3) using parameter values  $\beta = 0$ ,  $\varepsilon = 0.01$ ,  $D = 150$ , with  $\tau_0$  as indicated on the horizontal axis. Solid curve is given by (95). Dashed curve is obtained by numerically integrating (3) up to  $t = 10^6$  starting with initial conditions (98).

and then

$$\int_{-\infty}^{\infty} U_y^2 dy = \frac{4}{3}; \quad \int_{u_-}^{u_+} f_w du = 2; \quad (92)$$

$$\left( g_w - \frac{f_w}{f_u} g_u \right) \Big|_{u=u_\pm, w=w_0} = -\frac{1}{4} \quad (93)$$

so that the necessary conditions (14) hold, provided that  $|\beta| < 1$ . Applying Principal Result 2.1 to the cubic model, we obtain the amplitude equation, given by (4). As mentioned in §2, depending on the values of  $\tau_0$  and  $\beta$ , several different behaviours are possible. For the cubic model (3) we summarize this as follows.

**Proposition 4.1** *Consider a single interface solution of the form (7) for the cubic system (3). Define*

$$\beta_1 := \frac{3}{15} + \frac{2\sqrt{6}}{15} \approx 0.52659 \quad \text{and} \quad \beta_2 := \frac{1}{\sqrt{3}} \approx 0.57735$$

*The system (3) exhibits the following three distinct regimes:*

1. *If  $|\beta| < \beta_1$  then define*

$$\tau_{0h} := \frac{1}{2 - 6\beta^2}; \quad \tau_{0c} := \frac{1}{\frac{1}{2} + 3|\beta| - \frac{15}{2}\beta^2}. \quad (94)$$

- (a) *If  $\tau_0 < \tau_{0h}$  then  $l \rightarrow l_0$  in the limit  $\hat{t} \gg 1$ .*
- (b) *If  $\tau_0 \in (\tau_{0h}, \tau_{0c})$  then, in the limit  $\hat{t} \gg 1$ , the interface exhibits periodic oscillations of the form*

$$l(t) \sim l_0 + A_\infty \cos(\sqrt{3/\tau_0} \varepsilon D^{-1/2} t + \phi_0)$$

*where*

$$A_\infty = \sqrt{\frac{1}{3}(1 - 3\beta^2) - \frac{1}{6\tau_0}}. \quad (95)$$

- (c) *If  $\tau_0 > \tau_{0c}$  then eventually the interface merges with the boundary and no periodic oscillations occur.*

2. If  $|\beta| \in (\beta_1, \beta_2)$ , then define  $\tau_{0h}$  as in (94) and  $\tau_{0c} = \infty$ . Case 1(a) and (b) from above hold.
3. If  $|\beta| > \beta_2$ , then  $l \rightarrow l_0$  in the limit  $\hat{t} \gg 1$ , for all  $\tau_0 > 0$ .

The Principal Result 3.1 for two interfaces then yields:

$$\frac{dx_0}{d\hat{t}} = -\frac{3}{2}x_0 \left( \frac{A^2}{2} + l_0^2 \right) \quad (96)$$

$$\frac{dA}{d\hat{t}} = \left( \frac{1}{4}(1 - 3\beta^2) - \frac{1}{8\tau_0} - \frac{3}{2}x_0^2 \right) A - \frac{3}{4}A^3 \quad (97)$$

The result for a single interface is the same except that  $x_0$  is replaced by zero. The same results as in Proposition 4.1 also hold for two interfaces.

## 4.2 BACOL

The numerical software that we use for the treatment of the cubic model is a recently developed package called BACOL (see [42, 43, 44]). The approximate solution is a piecewise polynomial expressed as a linear combination of B-spline basis functions with time dependent coefficients. For the discretization of the spatial domain, this software employs B-spline collocation based on a mesh of points that partitions the spatial domain. This discretization process approximates the PDE by a system of time dependent ODEs that together with the boundary conditions can be described as a system of differential algebraic equations (DAEs). BACOL solves this DAE system using a well-known DAE solver called DASSL [3]. DASSL computes the approximation for the time-dependent B-spline coefficients. A significant feature of the software is that it employs adaptive control of estimates of the spatial and temporal errors. DASSL estimates the temporal error for each time step and adjusts the stepsize or order of accuracy of the time stepping formula so that this estimate is less than the user tolerance. BACOL computes a high order estimate of the spatial error of the collocation solution and adapts the spatial mesh based on an equidistribution principle so that the spatial error estimate is less than the user tolerance. The adaptive error control allows the software to efficiently compute numerical solutions that exhibit sharp transient regions in time or space. We will apply the results given in the previous sections to a particular model, then compare to the numerically computed solutions obtained using BACOL.

## 4.3 Numerical simulations

We now examine our results and compare with the numerically computed solution. First, we consider the single interface, then the two-interface solution.

**Experiment 1: Single interface,  $\beta = 0$ .** We took  $\beta = 0$ ,  $\varepsilon = 0.01$ ,  $D = 150$  so that  $l_0 = 1/2$ . Proposition 4.1 yields  $\tau_{0h} = \frac{1}{2}$ ,  $\tau_{0c} = 2$ , so that for  $\frac{1}{2} < \tau_0 < 2$ , the interface oscillates and approaches an amplitude of  $A_\infty = \sqrt{\frac{1}{3} - \frac{1}{6\tau_0}}$ . We then computed the evolution of (3) starting with the initial conditions given by

$$u(x, 0) = -\tanh\left(\frac{x - l_0 - 0.1}{\varepsilon}\right), \quad w(x, 0) = 0.01. \quad (98)$$

The evolution is shown as a contour plot in Figure 1(c,e) along with the amplitude  $A$  as determined by (4) and the location of the interface  $l$  as determined by (15).

**Experiment 2: Single interface,  $\beta = 0.1$ .** We now illustrate the three behaviours of the solution given by Proposition 4.1, and compare it with numerical simulation. We took  $\beta = 0.1$ ,  $\varepsilon = 0.001$  and  $D = 150$ , so that  $l_0 = 0.55$ . Proposition 4.1 yields  $\tau_{0h} = 0.5155$ ,  $\tau_{0c} = 1.379$ , so that for  $0.5155 < \tau_0 < 1.379$ , the interface oscillates and approaches an amplitude of  $A_\infty = \sqrt{0.3233 - \frac{1}{6\tau_0}}$ . For  $\tau_0 < 0.5155$ , the oscillations eventually die out leading to a stable interface located at  $l_0$ , whereas for  $\tau_0 > 1.379$ , the interface eventually hits the boundary. These three possible behaviours are illustrated in Figure 2. In Figure 2(a) we took  $\tau_0 = 0.4 < \tau_{0h}$ . As expected, the oscillations damp out leading to a stable interface located at  $l_0 = 0.55$ . In Figure 2(b) we took  $\tau_0 = 1$  so that  $\tau_{0h} < \tau_0 < \tau_{0c}$ . After a long transient, the

converges to a periodically oscillating interface whose amplitude approaches  $A_\infty \approx 0.3958$ . Finally in Figure 2(c), we have taken  $\tau_0 = 3 > \tau_{0c}$ . As expected, the interface eventually merges with the boundary and disappears.

**Experiment 3: Single interface,  $\beta = 0.5$ .** Similar to Experiment 2, we took  $\beta = 0.5$ ,  $\varepsilon = 0.001$  and  $D = 80$ , so that  $l_0 = 0.75$ . Here, we have taken the initial conditions as

$$u(x, 0) = -\tanh\left(\frac{x - l_0 - 0.01}{\varepsilon}\right), \quad w(x, 0) = 0.01. \quad (99)$$

Proposition 4.1 yields  $\tau_{0h} = 2$ ,  $\tau_{0c} = 8$ , so that for  $2 < \tau_0 < 8$ , the interface oscillates and approaches an amplitude of  $A_\infty = \sqrt{0.0833 - \frac{1}{6\tau_0}}$ . Figure 3 demonstrates the same three behaviours as given in Figure 2.

**Experiment 4: Single interface, Hopf bifurcation structure.** In this experiment, we compare the predicted value of  $A_\infty$  given by (95) with the value obtained from numerical simulations. We take  $\beta = 0$ ,  $\varepsilon = 0.01$ , and vary  $\tau_0$  from 0.2 to 0.75. For each fixed value of  $\tau_0$  in that range, we fully solve the system (3) until time  $t = 10^6$  and then read off the amplitude at that time. The resulting bifurcation diagram is shown in Figure 4. As expected, a good agreement is observed. Also as expected, the agreement with the numerical results is poor very close to the bifurcation point  $\tau_0 = 1/2$ : near the bifurcation, the amplitude changes very slowly. If we were to continue the numerical computation, in this case, for larger  $t$  values, we would see better agreement near  $\tau_0 = 0.5$  in Figure 4.

**Experiment 5: Two interfaces,  $\beta = 0$ .** Here, we consider the two-interface solution on the domain  $[-1, 1]$ . We take  $\varepsilon = 0.01$ ,  $D = 150$ ,  $\beta = 0$ , and  $\tau_0 = 1$ . For initial conditions, we take

$$u(x, 0) = \tanh\left(\frac{x - (-0.4)}{\varepsilon}\right) - \tanh\left(\frac{x - 0.8}{\varepsilon}\right) - 1, \quad w(x, 0) = 0.01.$$

so that the initial conditions correspond to two interfaces located at  $-0.4$  and  $+0.8$ . Figure 1(d,f) shows the numerical computations as well as the theoretical prediction given by (96, 97) and  $l$  given by (15). Very good agreement is observed.

## 5 Discussion

In this paper, we have examined how a one or two-interface solution of (1) can have oscillatory behaviour for particular values of  $\tau$ . We also found that the oscillations correspond to a supercritical Hopf bifurcation, provided that the conditions (14) hold. These conditions are the same ones that are needed to guarantee the existence and stability of a single interface for when  $\tau = 0$  [28]. The determination of this supercritical Hopf bifurcation was done by studying the ODE that describes the amplitude of the oscillations. This was accomplished through reducing the original PDE system to a system consisting of an ODE and a PDE, and then reducing this system to a system of ODEs. Finally, reducing the system of ODEs to a second order ODE, we performed a multiple scales analysis to determine an equation for the amplitude of the oscillations of the sharp interfaces of the solution of  $u$ . When comparing this asymptotic result with numerical simulation of the full system, excellent agreement was observed.

We found that no oscillations exist when  $\tau < O(\varepsilon/D)$ , either for one or two-interface solutions. For a solution which consists of two interfaces (also called a box or mesa solution), it was shown in [28] that even when  $\tau = 0$ , a two-interface solution is stable provided that  $1 \ll \ln(D) \ll 1/\varepsilon$  but is destabilized when  $D$  becomes exponentially large in  $\varepsilon$ . Such instability is due to a positive (but real) small eigenvalue that arises due to translation invariance; it induces a monotonic motion of the mesa towards one of the boundaries. On the other hand, we have implicitly assumed in this work that  $\ln(D) \ll 1/\varepsilon$ , so that the boundary terms in (26) were discarded. It is an open question to elucidate how the results in this paper would change if  $\ln(D)$  becomes sufficiently big, or equivalently, when interface inter-distance  $2l_0$  becomes sufficiently small.

For some parameter regimes, oscillations can eventually exceed domain size (see for example Proposition 4.1, subcase (c) and the accompanying Figures 2(c), 3(c)). Numerically, when the interface collides with the boundary, it typically disappears and the system gets “reset” to a nearly-uniform steady state. A natural question is whether this can lead to “chaos” via a subsequent destabilization of the homogeneous steady state through a Turing instability. We have found that this is not the case for the variety of models we tried. For example, it is easy to show that no Turing instability is possible when  $g(u, w) = g(u)$ , as is the case of the cubic model (3). But more generally, we cannot rule out such a “chaos loop”, although we have been unable to reproduce it.

We have shown that an unstable two-interface solution exhibits *in-phase* oscillations, whereby the two interfaces eventually oscillate in opposite directions about the center of the domain (also so-called breather instability). On the other hand, numerical simulations in [14] show that a different mode of instability is also possible when the two interfaces are close together; namely the two interfaces can exhibit *out-of-phase* oscillations, whereby they oscillate in the same direction. We think that this effectively corresponds to the regime where the two interfaces interact sufficiently strongly or where the interfaces interact with the boundary, and this interaction must be taken into account. It remains an open question to study this regime asymptotically.

Numerically, tracking the interface oscillations is a challenging problem. This is because there are two different temporal scales as well as two spatial scales. The software that we employ for the computation of the numerical solutions features adaptive error control in time and space and is therefore able to efficiently and accurately compute a numerical solution even when it exhibits rapid changes.

It would be interesting to expand this work for solutions consisting of more than two interfaces. Indeed, the symmetrical oscillations of a single interface on the domain of size 1 can be trivially extended by reflections to a  $K$  interface solution on the domain of size  $K$ . However there are other oscillatory modes that could potentially lead to an instability (there are as many modes as there are interfaces). Which mode dominates for  $K$  interfaces is an open question. Finally, the analogous oscillations in two or higher dimensions remain unexplored.

## 6 Acknowledgements

T.K. and P.M would like to thank the support from the NSERC Discovery grant program, Canada.

## References

- [1] M. Banerjee and S. Petrovski, Self-organised spatial patterns and chaos in a ratio-dependent predator–prey system, *Theor Ecol* (2011) 4:37–53.
- [2] C.M. Bender and S.A. Orszag. *Advanced mathematical methods for scientists and engineers*, Springer, 1999.
- [3] K.E. Brenan, S.L.Campbell, and L.R. Petzold. *Numerical solution of initial-value problems in differential-algebraic equations*, Classics in Applied Mathematics, Vol. 14, SIAM: Philadelphia, PA, 1996.
- [4] W. Chen and M.J. Ward. Oscillatory instabilities and dynamics of multi-spike patterns for the one-dimensional Gray-Scott model. *European Journal of Applied Mathematics*, 20:187-214, 2009.
- [5] W. Chen and M.J. Ward. The stability and dynamics of localized spot patterns in the two-dimensional Gray-Scott model. submitted to *SIAM J. Appl. Dynam. Systems*, 2010.
- [6] A. Doelman, B. Sandstede, A. Scheel, G. Schneider, The dynamics of modulated wave trains, *Mem. Amer. Math. Soc.* 199 (2009).
- [7] S. Ei, H. Ikeda and T. Kawana. Dynamics of front solutions in a specific reaction-diffusion system in one dimension. *Japan J. Indust. Appl. Math.* 25:117-147, 2008.

- [8] S. Ei, H. Ikeda and T. Kawana, Dynamics of front solutions in a specific reaction-diffusion system in one dimension, *Japan J. Indust. Appl. Math.* (2008) 25:117-147
- [9] R. E. Goldstein, D. J. Muraki, and D. M. Petrich. Interface proliferation and the growth of labyrinths in a reaction-diffusion system. *Phys. Rev. E*, 53(4):3933–3957, 1996.
- [10] S.V. Gurevich, Sh. Amiranashvili and H.G. Purwins. Breathing dissipative solitons in three component reaction-diffusion system. *Physical Review E*. 74, 2006.
- [11] A. Hagberg and E. Meron. Pattern formation in non-gradient reaction-diffusion systems: the effect of front bifurcations. *Nonlinearity*, 7:805-835, 1994.
- [12] P. van Heijster, A. Doelman and T.J. Kaper. Pulse Dynamics in a Three-Component System: Stability and bifurcations. *Physica D*, 237:3335-3368, 2008.
- [13] D. Haim, G. Li, Q. Ouyang, W.D. McCormick, H.L. Swinney, A. Hagberg and E. Meron. Breathing spots in a reaction-diffusion system. *Phys. Rev. Lett.*, 77:190-193, 1996.
- [14] T. Ikeda and Y. Nishiura. Pattern selection for two breathers. *SIAM J. Appl. Math.*, 54(1):195-230, 1994.
- [15] H. Ikeda and T. Ikeda. Bifurcation phenomena from standing pulse solutions in some reaction-diffusion systems. *J. Dyn. Diff. Eqns.* 12(1), 2000.
- [16] A. Kaminaga, V.K. Vanag, and I.R. Epstein, A Reaction–Diffusion Memory Device, *Angewandte Chemie*, 45, 3087 (2006).
- [17] R. Kapral and K. Showalter, editors. *Chemical waves and patterns*. Kluwer, Dordrecht, 1995.
- [18] B. S. Kerner and V. V. Osipov. *Autosolitons: a New Approach to Problems of Self-Organization and Turbulence*. Kluwer, Dordrecht, 1994.
- [19] A. J. Koch and H. Meinhardt. Biological pattern formation: from basic mechanisms to complex structures. *Rev. Modern Physics*, 66(4):1481–1507, 1994.
- [20] S. Koga and Y. Kuramoto. Localized Patterns in Reaction-Diffusion Systems. *Progress of Theoretical Physics*. 63(1):106–121, 1980.
- [21] T. Kolokolnikov and M. Tlidi, Spot deformation and replication in the two-dimensional Belousov-Zhabotinski reaction-diffusion system, *Physical Review Letters*, Vol.98 2007(18), article 188303.
- [22] T. Kolokolnikov, T. Erneux, and J. Wei. Mesa-type patterns in the one-dimensional Brusselator and their stability. *Physica D*, 214:63–77, 2006.
- [23] T. Kolokolnikov, M. Ward, and J. Wei. Self-replication of mesa patterns in reaction-diffusion models. *Physica D*, Vol. 236(2):104–122, 2007.
- [24] T. Kolokolnikov, M.J. Ward and J. Wei. Slow transitional instabilities of spike patterns in the one-dimensional Gray-Scott model. *Interfaces and Free Boundaries*. 8(2):185-222, 2006.
- [25] Y. Kuramoto. *Chemical Oscillations, Waves and Turbulence*. Springer-Verlag, Berlin, 1984.
- [26] I Lengyel and IR Epstein. Modeling of Turing structures in the chlorite-iodide-malonic acid-starch reaction system. *Science*, Vol. 251(4994):650–652, 1991.
- [27] H. Meinhardt. *Models of biological pattern formation*, Academic press, London, 1982.
- [28] R.C. McKay and T. Kolokolnikov. Instability thresholds and dynamics of mesa patterns in reaction-diffusion systems. submitted, *Discrete and Continuous Dynamical Systems - B*, 2011.

- [29] C. B. Muratov and V. Osipov. Scenarios of domain pattern formation in a reaction-diffusion system. *Phys.Rev.E*, 54:4860–4879, 1996.
- [30] C. B. Muratov. Synchronization, chaos, and breakdown of collective domain oscillations in reaction-diffusion systems. *Phys.Rev.E*, 55:1463–1477, 1997.
- [31] C. Muratov and V. V. Osipov. General theory of instabilities for patterns with sharp interfaces in reaction-diffusion systems. *Phys, Rev. E*, 53(4):3101-3116, 1996.
- [32] J. D. Murray. *Mathematical Biology*. Springer-Verlag, Berlin, 1989.
- [33] M. Nagayama, K.-I. Ueda, and M. Yadome. Numerical approach to transient dynamics of oscillatory pulses in a bistable reaction-diffusion system. *Japan J. Indust. Appl. Math.* 27:295–322, 2010.
- [34] W. Ni and M. Tang. Turing patterns in the Lengyel-Epstein system for the CIMA reaction. *Trans. AMS*, 357(10):3953–3969, 2005.
- [35] Y. Nishiura and H. Fujii. Stability of singularly perturbed solutions to systems of reaction-diffusion equations. *SIAM J.Math.Anal.*, 18:1726–1770, 1987.
- [36] Y. Nishiura and M. Mimura. Layer oscillations in reaction-diffusion systems. *SIAM J.Appl. Math.*, 49:481–514, 1989.
- [37] J.E. Pearson. Complex patterns in a simple system. *Science*. 261(5118):189-192, 1993.
- [38] M. Suzuki, T. Ohta, M. Mimura and H. Sakaguchi. Breathing and wiggling motions in three-species laterally inhibitory systems. *Physical Review E*, 52(4):3645–3655, 1995.
- [39] M. Taki, M. Tlidi and T. Kolokolnikov, editors. Dissipative localized structures in extended systems. *Chaos Focus issue*, 17, 2007.
- [40] V.K. Vanag and I.R. Epstein. Localized patterns in reaction-diffusion systems. *Chaos*, Vol.17, No.3, 2007.
- [41] V. Volpert and S. Petrovskii, Reaction–diffusion waves in biology, *Physics of Life Reviews* 6 (2009) 267–310.
- [42] R. Wang, P. Keast and P. Muir. A comparison of adaptive software for 1-D parabolic PDEs. *J. Comput. Appl. Math.*, 169(1): 127–150, 2004.
- [43] R. Wang, P. Keast and P. Muir. A high-order global spatially adaptive collocation method for 1-D parabolic PDEs. *Applied Numerical Mathematics*, 50(2):239–260, 2004.
- [44] R. Wang, P. Keast and P. Muir. BACOL: B-Spline Adaptive COLlocation Software for 1-D Parabolic PDES. *ACM Transactions on Mathematical Software*, 30(4):454–470, 2004.
- [45] M.J. Ward and J. Wei. Hopf bifurcation and oscillatory instabilities of spike solutions for the one-dimensional Gierer-Meinhardt model. *J. Nonlinear Science*, 13(2):209-264, 2003.
- [46] H. Yizhaq and E. Gilad, Localized structures in dryland vegetation: forms and functions, *Chaos*, 17, 037109 (2007)